Separation Science and Technology
Publication details, including instructions for authors and subscription information:
http://www.informaworld.com/smpp/title~content=t713708471

Overload Quasi-Static Linear Gradient Chromatography: Theory Versus Hydroxyapatite High-Performance Liquid Chromatography

Tsutomu Kawasaki[a]; Makoto Niikura[a]
[a] CHROMATOGRAPHIC RESEARCH LABORATORY KOKEN BIOSCIENCE INSTITUTE, TOKYO, JAPAN

To cite this Article Kawasaki, Tsutomu and Niikura, Makoto(1990) 'Overload Quasi-Static Linear Gradient Chromatography: Theory Versus Hydroxyapatite High-Performance Liquid Chromatography', Separation Science and Technology, 25: 4, 397 — 435
To link to this Article: DOI: 10.1080/01496399008050341
URL: http://dx.doi.org/10.1080/01496399008050341

SEPARATION SCIENCE AND TECHNOLOGY, 25(4), pp. 397-435, 1990

Overload Quasi-Static Linear Gradient Chromatography: Theory Versus Hydroxyapatite High-Performance Liquid Chromatography

TSUTOMU KAWASAKI and MAKOTO NIIKURA

CHROMATOGRAPHIC RESEARCH LABORATORY
KOKEN BIOSCIENCE INSTITUTE
3-5-18 SHIMO-OCHIAI, SHINJUKU-KU, TOKYO 161, JAPAN

Abstract

The earlier theory of quasi-static linear gradient chromatography under overload conditions is improved. The quasi-crystalline phase model for the molecules adsorbed on the adsorbent surfaces in the column is specified; this model was introduced earlier, and it is used in the present theory. A close experimental verification of the theory is carried out for the case of hydroxyapatite high-performance liquid chromatography using both turkey and chicken egg white lysozymes as probes. It can be deduced that a quasi-crystalline phase of lysozyme molecules, in fact, is realized on the hydroxyapatite surfaces in the column. The mutual interaction energy per molecule of lysozyme occurring provided the maximum possible contact with other molecules is made on the hydroxyapatite surface can be estimated to be larger than 0.2–0.4 kcal/mol.

INTRODUCTION*

Earlier (*1–3*), the approximate theory of quasi-static linear gradient chromatography under overload conditions was developed for a mixture of molecules with the same dimensions and the same shape, taking into

*Abbreviations. HA, hydroxyapatite. HPLC, high-performance liquid chromatography. ϕ, inside column diameter. Buffer A, potassium phosphate buffer at pH $\approx$ 6.8. P, pressure drop. T, temperature.

account both the mutual interactions among molecules occurring on the adsorbent surface and the longitudinal diffusion in the column. The first purpose of the present work is to slightly modify this theory and to specify it in order for it to be compatible with the new concepts that are involved in the general theory of quasi-static linear gradient chromatography with small sample loads that has been developed recently (*4–6*); the relationship between the overload theory (*1–3*) and the small load theory (*4–6*) is argued in detail in Ref. *6*. The second purpose is to give a close experimental verification of the specified overload theory for the case of hydroxyapatite (HA) high-performance liquid chromatography (HPLC) by using both turkey and chicken egg white lysozymes as probes.

In another series of papers (*7–11*), the fundamental mechanism of overload gradient chromatography was explored by using an ideal molecular model with infinite dimensions. Especially in Ref. *11*, the work (*7–10*) was improved and specified in order for it to be compatible with the new concepts that are involved in the theory in Refs. *4–6*; this gives the foundation of the present work. Thus, an important conclusion was attained in Ref. *11* that the molecules adsorbed on the absorbent surfaces in the column under overload conditions are usually repulsively interacting with one another, and that the total shape of the chromatogram strongly depends upon what type of phase is realized by the molecules adsorbed on the adsorbent surface. Especially with molecules with an asymmetrical shape such as those represented by a rod or a prolate spheroid [most of the protein molecules are more or less asymmetrical in shape, and a lysozyme molecule can approximately be represented by a prolate spheroid of dimensions $45 \times 30 \times 30$ Å (*12*)], two models were proposed for the phase of the molecules realized on the adsorbent surface (*11*). Thus, in the first model (called an amorphous phase model), the molecules are situated *at random* on the adsorbent surface, maintaining a parallel orientation with one another (see below), whereas in the second (called a quasi-crystalline phase model), the positions of the molecules (arranged in parallel with one another) are *restricted* to one another due to the energetic interaction among them through the side of the rod (or the prolate spheroid); on the basis of statistical-mechanical consideration, it can, in general, be assumed that the molecules (with a more or less elongated shape) are arranged in parallel with one another on the adsorbent surface in order to avoid the mutually superimposed state, provided the molecular density on the adsorbent surface is high enough (for details, see Ref. *11*). Further, by introducing the competition model for the adsorption and desorption phenomena occurring in the column, it was concluded (*11*) that a chromatogram rectangular in shape is obtained provided the amorphous

phase is realized on the adsorbent surface whereas a right-angled-triangular chromatogram with tailing is obtained provided the quasi-crystalline phase is realized; the competition model states that sample molecules (with adsorption groups) and particular ions from the buffer constituting the molarity gradient compete for adsorption on the sites that are arranged in some manner on the surfaces of the packed particles in the column (for details, see Ref. *11*). The fact that chromatograms with a shape close to a right-angled triangle with tailing are often experienced under overload conditions implies that the quasi-crystalline phase is realized in many actual instances (*11*).

In Appendix I, the quasi-crystalline phase model is specified. In Appendix II, we mention how the present theory, in which both the amorphous and the quasi-crystalline phase models are introduced, approaches the theory of the earlier paper (*11*) when the dimensions of the sample molecules increase and approach infinity.

In the present work, by comparing the new theory with the experiment, it is deduced that a quasi-crystalline phase, in fact, is realized on the HA surfaces in the column with both turkey and chicken lysozymes as well as with a mixture of them; the interaction energy per molecule of lysozyme occurring, provided the maximum possible contact with other molecules is made on the HA surface, can be estimated to be larger than 0.2–0.4 kcal/mol.

In the introductory part of an earlier paper (*13*), the concrete structure and the arrangement of the adsorbing sites on the crystal surface of HA are mentioned. Thus, it can be deduced (*13*) that two types of main surface [**a** (or **b**) and **c** surfaces] appear on a crystal. On the **c** surface, negatively charged adsorbing sites (called P sites) are arranged in a hexagonal manner with the minimal interdistance equal to 9.42 Å (*13*). Lysozyme molecules (with a basic isoelectric point) are adsorbed onto P sites by using positively charged adsorption groups (ε−amino and guanidinyl groups) that are arranged in some manner on the molecular surface (*13, 14*). Potassium ions from the Buffer A molarity gradient [for Buffer A, see Experimental Section (A)] are also adsorbed onto P sites, and competition occurs between lysozyme molecules and potassium ions from the buffer for adsorption onto P sites.

The parameters m, g', etc. appearing in the Theoretical Section are therefore concerned with potassium ions from the buffer. Nevertheless, in the Experimental Section, the experimental data will be expressed by using the parameters concerning phosphate ions from the buffer (with values 2/3 times as large as those for potassium ions), in accordance with the common practice. In fact, molecules with an acidic isoelectric point

are usually absorbed onto positively charged adsorbing sites (called C sites) that are arranged on the **a** (or **b**) crystal surface of HA, and they compete with phosphate ions from the buffer for adsorption (*13*). In order to arrange all the chromatographic data (including those for molecules with unknown isoelectric points), it is convenient to apply the commonly used expression of the parameters.

THEORETICAL

(A) Theoretical Chromatogram in the Absence of Longitudinal Diffusion in the Column

In the Ref. *6* Appendix the general theory of quasi-static linear gradient chromatography with small sample loads is summarized.

Equations (A1)-(A18) in the Ref. *6* Appendix are even valid under overload conditions where mutual molecular interactions occur on the adsorbent surfaces in the column [see Ref. *6*, Discussion Section (B)], of which Eq. (A17) (under overload conditions) can be rewritten as simultaneous equations for the respective components (1, 2, . . . , ρ) of the sample mixture as

$$\overrightarrow{\mathrm{div}_s}\left[\frac{B_{(\rho')}(m, \chi_{(1)}, \chi_{(2)}, \ldots, \chi_{(\rho)})}{1 - B_{(\rho')}(m, \chi_{(1)}, \chi_{(2)}, \ldots, \chi_{(\rho)})} \cdot \chi_{(\rho')}\right] + \frac{\partial \chi_{(\rho')}}{\partial m} = 0$$

$$(\rho' = 1, 2, \ldots, \rho) \qquad (1)$$

In Eq. (1), $\chi_{(\rho')}$ (where $\rho' = 1, 2, \ldots, \rho$) represents the molecular density of component ρ' of the sample mixture on the adsorbent surface; m is the molarity of the gradient element (i.e., substances constituting the gradient) in the column; $B_{(\rho')}(m, \chi_{(1)}, \chi_{(2)}, \ldots, \chi_{(\rho)})$ is the partition of component ρ' in the mobile phase in a vertical column section, or the ratio of the amount of molecules in the mobile phase to the total amount of component ρ' in that column section; and s is defined as

$$s = gL \qquad (2)$$

where L and g represent the length of the column and the slope of the molarity gradient, respectively. g is expressed as an increase in molarity per unit length of the column measured from the outlet to the inlet of the column in order for s to have a dimension of molarity. [In the earlier papers (*4–6*), s is defined as the product of the slope, g', of the gradient expressed as an increase in molarity per unit interstitial volume of the column and the total interstitial volumes, L', of the column. It is evident that $g'L' = gL$.] The molecular flux participating in Eq. (1) is called the intermediate abstract flux (*3*), and Eq. (1) represents the fundamental simultaneous continuity equations both in the presence of mutual molecular interaction on the adsorbent surface and in the absence of longitudinal diffusion in the column (*3, 6*).

Under Approximations (a)–(d) in the Ref. *11* Theoretical Section (B), Eq. (1) reduces to Eq. (1) in Ref. *3* (which also appears as Eq. 39 in Ref. *11*), or to

$$\operatorname{div}_s \left[\frac{\overrightarrow{B_{(\rho')}(m, \chi)}}{1 - B_{(\rho')}(m,\chi)} \cdot \chi_{(\rho')} \right] + \frac{\partial \chi_{(\rho')}}{\partial m} = 0 \qquad (\rho' = 1, 2, \ldots, \rho) \qquad (3)$$

in which

$$\chi = \sum_{\rho''=1}^{\rho} \chi_{(\rho'')} \qquad (4)$$

represents the total molecular density on the adsorbent surface, being normalized in order for it to be comprised between 0 and 1.

In Ref. *3*, by introducing the competition model (Introduction Section), the theoretical chromatogram $\hat{f}_{(\rho'),s}(m)$, for a component ρ' of the mixture of molecules with the same dimensions and the same shape has been calculated on the basis of Eq. (3). For this calculation an assumption is used that a molecular band with an infinitesimal width is formed initially at the inlet of the column (see Ref. *3*). This assumption, although untrue, is reasonable for the final result of the calculation since the width of the molecular band occurring during its migration on the column (to be precise, the migration on the hypothetical column with an infinite length) is usually much larger than the width of the initial band occurring in the vicinity of the column inlet. In the present work the calculation method in Ref. *3* is slightly modified by replacing the parameter s (Eq. 2) with the new parameter $\dot{s}$, defined as

$$\dot{s} = g\dot{L} \qquad (5)$$

in which $\dot{L}$ represents the distance between the center of the initial molecular band with a finite width (occurring in the vicinity of the column inlet) and the outlet of the column. With this modification the theoretical chromatogram (Eqs. 43 and 44 in Ref. *3*, or Eqs. 3 and 4 in Ref. *2*) can be rewritten as

$$\hat{f}_{(\rho'),s'}(m) = \frac{1}{\sum_{\rho''=1}^{\rho} \chi^*_{(\rho'')}} \cdot \frac{(\varphi m + 1)^{x'}}{q_{(\rho')s'}} \cdot \left(\frac{dY_{(\rho')}(\chi_{(\rho')})}{d\chi_{(\rho')}}\right)^2 \left(\frac{d^2Y_{(\rho')}(\chi_{(\rho')})}{d\chi^2_{(\rho')}}\right)^{-1} \tag{6}$$

and

$$m = \frac{1}{\varphi} \cdot \{[(x' + 1)\phi q_{(\rho')s'} \cdot \left(\frac{dY_{(\rho')}(\chi_{(\rho')})}{d\chi_{(\rho')}}\right)^{-1} + (\varphi m_{in} + 1)^{x'+1}]^{1/(x'+1)} - 1\} \tag{7}$$

where $\chi_{(\rho')}$ plays the role of an intermediate parameter. The term $1/\Sigma^{\rho}_{\rho''=1}\chi^*_{(\rho'')}$ on the right-hand side of Eq. (6) (which does not appear in Eq. 43 in Ref. *3* that corresponds to Eq. 6) is to normalize the total chromatogram, $\Sigma^{\rho}_{\rho'=1} \hat{f}_{(\rho'),s'}(m)$, such that

$$\int_{m_{in}}^{\infty} \left[\sum_{\rho'=1}^{\rho} \hat{f}_{(\rho'),s'}(m)\right] dm = 1 \tag{8}$$

In both Eqs. (6) and (7), φ represents a positive constant characterizing the competing ions constituting the molarity gradient in the column. x' is the number of adsorbing sites on the adsorbent surface on which the adsorption of competing ions is impossible due to the presence of an adsorbed molecule; x' therefore represents the effective dimensions of the molecule assumed to be the same for any component of the mixture. $\chi^*_{(1)}, \ldots, \chi^*_{(\rho'')}, \ldots, \chi^*_{(\rho)}$ [which are also involved in the function $Y_{(\rho')}(\chi_{(\rho')})$ as parameters; see below], respectively, are the amounts of components $1, \ldots, \rho'', \ldots, \rho$ loaded initially on the column, expressed in a unit such that $\chi^*_{(\rho'')} = 1$ provided the whole column is saturated only with component ρ''. m_{in} is

the initial molarity of competing ions at the beginning of the gradient. $q_{(\rho')}$ is defined as

$$q_{(\rho')} = \beta\tau_{(\rho')}e^{\hat{E}_{(\rho')}/kT} \tag{9}$$

in which $E_{(\rho')}$ represents the absolute value of the interaction energy with adsorbing site(s) per molecule of component ρ' occurring provided the molecule is isolated on the adsorbent surface (for details, see Refs. *15* and *16*); $\tau_{(\rho')}$, the configurational entropy factor per molecule of component ρ' occurring provided the molecule is isolated on the adsorbent surface (for details, see Refs. *15* and *16*); and β, a positive constant related to the property of the column (for details see Ref. *17*).

The function $Y_{(\rho')}(\chi_{(\rho')})$ in Eqs. (6) and (7) is defined as

$$Y_{(\rho')}(\chi_{(\rho')}) = H(\chi)\chi_{(\rho')} \tag{10}$$

in which

$$H(\chi) = \frac{e^{\hat{E}\zeta(\chi)/kT}}{p^*(\chi)} \tag{11}$$

and χ is represented as a function of $\chi_{(\rho')}$ a[r]

$$\chi\left(=\sum_{\rho''=1}^{\rho}\chi_{(\rho'')}\right) = \sum_{\rho''=1}^{\rho}\chi^*_{(\rho'')}\cdot\left[\frac{\chi_{(\rho')}}{\chi^*_{(\rho')}}\right]^{q_{(\rho')}/q_{(\rho'')}} \tag{12}$$

The function $H(\chi)$ (Eq. 11) is concerned with mutual molecular interactions occurring on the adsorbent surfaces in the column, the numerator and the denominator on the right-hand side of Eq. (11) representing the energetic and the geometrical interaction, respectively. Thus, $\hat{E}$ [which is equivalent with $x'_{(\rho')}\hat{\eta}$ in Ref. 11] represents the interaction energy (to be precise, the apparent interaction energy; see the Discussion Section) per molecule occurring provided the maximum possible contact with other molecules is made; in the usual case of repulsive interactions, $\hat{E} > 0$ (cf. the Introduction Section). The function $\zeta(\chi)$ can, in general, be assumed (*11*) to increase with an increase of χ, being equal to zero and unity when χ is zero and unity, respectively. [It should be noted that $\hat{E}\zeta(\chi)$ is equivalent

with $E^*_{(p')}(\chi)$ in Ref. *11*.] In Ref. *11*, two possible approximate forms of the function $\zeta(\chi)$:

$$\zeta(\chi) \approx \chi \tag{13}$$

and

$$\zeta(\chi) \approx \sqrt{\chi} \tag{14}$$

have been proposed. Equations (13) and (14) can be considered to hold provided the amorphous and the quasi-crystalline phase of the molecules are realized on the adsorbent surface, respectively [Introduction Section; for detail, see Discussion Section (A) in Ref. *11* and Appendix I]. Finally, the function $p^*(\chi)$ represents approximately the probability that, when a new molecule is added at random to the adsorbent surface, a proportion χ of which is already occupied by molecules, it is not superimposed on the already adsorbed molecules (for details, see Refs. *15* and *16*). Therefore, $p^*(\chi)$ can approximately be represented as

$$p^*(\chi) \approx 1 - \chi \tag{15}$$

The asymptotic expression of the theoretical chromatogram (Eqs. 6 and 7) occurring when $x' \approx \infty$ has been derived in Ref. *11* (see the Introduction Section); this is presented as Eqs. (A4a)–(A4c) in Appendix II.

(B) Approximate Expression of the Theoretical Chromatogram in the Presence of Longitudinal Diffusion in the Column

Both in the absence of mutual molecular interaction and in the presence of longitudinal diffusion in the column, the theoretical chromatogram for any component of the mixture can be calculated on the basis of Eq. (A21) in the Ref. *6* Appendix. The chromatogram, f^0, realized when a molecular band with an infinitesimal width is formed initially at the inlet of the column, can be represented in an approximate Gaussian form (Eq. 43 in Ref. *4*) which can be written as

$$f^0[m;\mu(s),\sigma(s;g)] = \frac{1}{\sqrt{2\pi}\sigma(s;g)} \cdot e^{-[m-\mu(s)]^2/[2[\sigma(s;g)]^2]} \tag{16}$$

where, by introducing the competition model (Introduction Section), $\mu(s)$ and $\sigma(s;g)$ can be represented as Eqs. (45) and (46) in Ref. *4*, or as

$$\mu(s) = \frac{1}{\varphi}\{[(x' + 1)\varphi q s + (\varphi m_{in} + 1)^{x'+1}]^{1/(x'+1)} - 1\} \qquad (17)$$

and

$$\sigma(s;g) = \sqrt{2g\Theta_0 s}\{1 + q[\phi\mu(s) + 1]^{-x'}\} \qquad (18)$$

respectively; the parameter Θ_0 (with a dimension of length) in Eq. (18) measures the longitudinal diffusion in the column. [In the earlier papers (*4–6*), the parameter $\Theta \equiv \Theta_0 g/g'$ was considered instead of Θ_0; for g', see the explanation of Eq. 2.] It can, in general, be assumed [see Ref. *5* Discussion Section (C)] that Θ_0 (or Θ) depends upon both the slope g (or g') of the molarity gradient and the type of the sample molecule. With a mixture of molecules with the same dimensions and the same shape, Θ_0 (or Θ) can be assumed to be independent of the molecular type, however [cf. Ref. *5* Discussion Section (C)].

As far as molecules with the same dimensions and the same shape are concerned, φ, m_{in}, g, x', and Θ_0 in both Eqs. (17) and (18) are constant, independent of the molecular type (for Θ_0, see above). This means that if q (which characterizes the molecular type) is given, then the chromatogram (Eq. 16) is determined. It should be noted, however, that if q is given, then μ is determined, and vice versa (see Eq. 17); this means that the chromatogram (Eq. 16) is determined if μ is given. Further, it is possible to consider that Eq. (16) represents *the molecular distribution occurring provoked by diffusion on the molarity gradient at "time" s* (second point of view on gradient chromatography) rather than the chromatogram (first point of view on gradient chromatography; for the two points of view, see Ref. *4* Appendix II), and that the extent of the molecular distribution is determined if the position, μ, *on the molarity gradient* is given. Therefore, writing $G_{s,g}[m;\mu,\sigma(\mu)]$ instead of $f^{\circ}[m;\mu(s),\sigma(s;g)]$, and replacing s by $\hat{s}$:

$$f_{(\rho'),\hat{s};g}(m) = \int_{m_{in}}^{\infty} \hat{f}_{(\rho'),\hat{s}}(\mu) G_{\hat{s};g}[m;\mu,\sigma(\mu)]\, d\mu \qquad (19)$$

would represent approximately the chromatogram for component ρ' of the mixture occurring in the presence of both mutual molecular interac-

tions on the adsorbent surfaces and longitudinal diffusion in the column. It is easy to show that Eq. (19) coincides with Eq. (16) [in which the parameter q is replaced by $q_{(\rho')}$; cf. Eqs. 17 and 18] at the limit of no molecular interactions with the infinitesimal sample load; this can be shown on the basis of the fact that Eqs. (43) and (44) in Ref. *3* [which are equivalent with Eqs. 6 and 7 except for the term $1/\Sigma_{\rho''=1}^{\rho} \chi_{(\rho'')}^{*}$ on the right-hand side of Eq. 6] converge into Eq. (31) in Ref. *3* at this limit.

The total chromatogram, $f_{s',g}(m)$, can be represented as

$$f_{s',g}(m) = \sum_{\rho'=1}^{\rho} f_{(\rho'),s',g}(m) \tag{20}$$

which is normalized such that

$$\int_{m_{in}}^{\infty} f_{s',g}(m)\, dm = 1 \tag{21}$$

It should be noted that Eq. (20) is the improved expression of Eq. (24) in an earlier paper (*2*).

EXPERIMENTAL

(A) Materials and Methods

Both spherical HA particles (with diameters of about 5 μm; cf. Refs. *18* and *19*) and HA-packed SUS316 stainless steel columns (KB columns; Koken Co. Ltd., Tokyo, Japan) were prepared in our laboratory. The inside column diameter was always 6 mm; lengths of 0.5, 1, 3, 10, and 30 cm were prepared. The 3-cm column was used as either a precolumn or a main column. If a large overall column length was necessary, it was provided by connecting 30-cm columns in series by using fine tubes.

The ratio of the void volume to the total packed volume of the HA crystals in the column was estimated by using the two following methods. Thus, in the first method, the dry weight of the packed crystals was estimated. The dry crystal volume was calculated on the basis of the crystal structure of HA [$Ca_{10}(PO_4)_6(OH)_2$; cf. Ref. *13*], and the ratio in question was estimated to be 0.798 from the dry crystal volume. In the second method, the time that is necessary for a pulse of sucrose solution to pass through a column was measured, and the ratio in question was estimated to be 0.823 on the basis of the assumption that the migration velocity of sucrose is equal to that of the solvent (water) (for details, see Ref. *20*). We will hereafter use the latter value of 0.823 for all the calculations.

The HPLC experiments were carried out by connecting the column to an HPLC pump. Thus, the sample molecules dissolved in 1 m*M* potassium phosphate buffer at pH ≈ 6.8 (i.e., an equimolar mixture of K_2HPO_4 and KH_2PO_4; called Buffer A. 1 m*M* is the value concerned with phosphate ion in the Buffer A.) was injected into the column (or the column system) by using the injector settled between the HPLC pump and the column inlet; this was followed by a rinsing process carried out by using the 1-m*M* Buffer A. During this process, virtually all the molecules (except denatured minor components) stayed in the stationary phase (i.e., on the surface of the adsorbent) in the vicinity of the column inlet, forming a band (cf. Fig. 1). Material was then eluted using a linear molarity gradient of Buffer A. The sample elution was monitored by measuring the ultraviolet absorption (at 280, 300, or 305 nm) in a flow cell. At the same

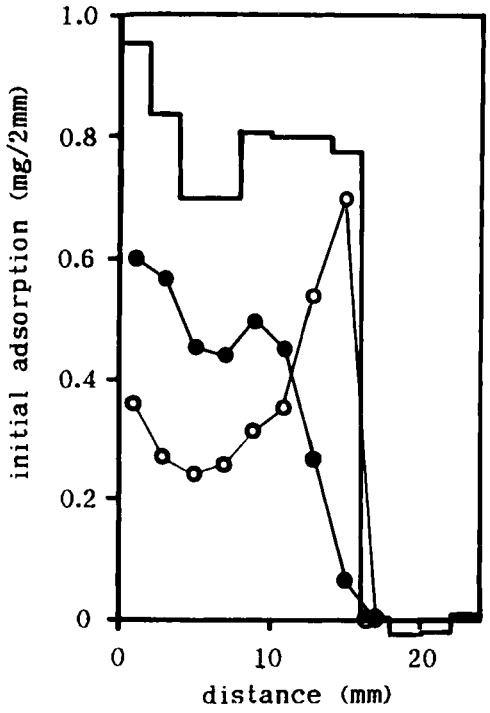

FIG. 1. The histogram shows the initial adsorption of a mixture of turkey (3.75 mg) and chicken (3.75 mg) egg white lysozymes in the column as a function of the distance from the column inlet. The two curves obtained by connecting the filled and unfilled circles represent the contributions of turkey and chicken lysozymes to the total chromatogram, respectively. For details, see text.

time, the molarity gradient was monitored by measuring the refractive index in a special flow cell with a low angle.

The width of the initial molecular band formed in the vicinity of the column inlet (see above) was estimated by the following way. Thus, by using the same method as in the case of chromatography (see above), the sample molecules dissolved in the 1-m*M* Buffer A was injected, with a flow rate of 0.5 mL/min, into a 3-cm column or 3-cm columns connected in series using fine tubes; this was followed by a rinsing process of 5–10 min carried out by using the 1-m*M* Buffer A. The column contents (i.e., HA particles) were extruded from the inlet of the column(s) by pushing them from the outlet with a rod. The cylindrical mass of the HA particles extruded from the column was cut into slices with a thickness of 2 mm; each of them was then suspended in 5 mL of 0.5 *M* Buffer A with agitation in order to dissolve the sample molecules that had been captured on the HA surfaces into solution. The suspension was centrifuged, and the optical density at 230 and/or 280 nm of the supernatant was measured in order to estimate the total amount of the sample molecules that had been present in the slice.

The sample molecules applied to the experiment were limited to both turkey egg white lysozyme (Sigma) and chicken egg white lysozyme (P. L. Biochemicals).

(B) Important Experimental Parameters

Experimental parameters which will play important roles are defined below.

$m_{(P)}$ and $m_{(K^+)}$: phosphate and potassium molarity in Buffer A, respectively. $m_{(K^+)}$ is 1.5 times as large as $m_{(P)}$.

$m_{elu(P)}$: elution phosphate molarity, i.e., the phosphate molarity in the Buffer A gradient at which the maximum height of the chromatographic peak is eluted.

$m_{in(P)}$: initial phosphate molarity, i.e., the phosphate molarity in Buffer A occurring before the Buffer A gradient begins.

$\sigma_{(P)}$: approximate standard deviation (with a dimension of m*M*) of the chromatographic peak measured in terms of the phosphate molarity range of the Buffer A gradient over which the peak appears. $\sigma_{(P)}$ is defined as the half-width at 0.6065 times the maximum height of the peak; this is exactly equal to the standard deviation provided the peak has a precise Gaussian shape.

L: total (overall) column length measured in centimeters.

$g'_{(P)}$ and $g'_{(P)}(\phi = 1\ \text{cm})$: $g'_{(P)}$ represents the slope concerning the phosphate molarity gradient in the Buffer A gradient, measured in unit of M/mL or mM/mL. $g'_{(P)}(\phi = 1\ \text{cm})$ represents the reduced $g'_{(P)}$ to inside column diameter $\phi = 1$ cm. $g'_{(P)}(\phi = 1\ \text{cm})$ is 0.36 ($= 0.6^2$) times as large as $g'_{(P)}$. g (cf. Eq. 2 and the last paragraph in the Introduction Section) can be written in terms of $g'_{(P)}(\phi = 1\ \text{cm})$ as

$$g = \frac{\pi}{4}(0.823)(1.5)g'_{(P)}(\phi = 1\ \text{cm})$$

$$= 0.970g'_{(P)}(\phi = 1\ \text{cm}) \tag{22}$$

where 0.823 represents the ratio of the void volume to the total packed volume of the HA crystals in the column [see Section (A)], and 1.5 is the molarity ratio between potassium and phosphate ions in Buffer A.

$s_{app(P)}$: product of $g'_{(P)}(\phi = 1\ \text{cm})$ and L. s (cf. Eq. 2) can be written in terms of $s_{app(P)}$ as

$$s = 0.970s_{app(P)} \tag{23}$$

q_{app}: experimental parameter related to q (cf. Eqs. 17 and 18) by the relationship

$$q = q_{app}/0.970 \tag{24}$$

(C) The Width of the Initial Molecular Band as a Function of Sample Load

For the calculation of the theoretical chromatogram under overload conditions [Section (E)], it is necessary to have knowledge of how $\chi^*_{(P')}$ (Eq. 12) and $\dot{s}$ (Eq. 5) change as functions of sample load. For this purpose it is sufficient to estimate the width of the initial molecular band occurring in the vicinity of the column inlet as a function of sample load.

The histogram in Fig. 1 shows a typical example of the initial adsorption of a mixture of turkey (3.75 mg) and chicken (3.75 mg) egg white lysozymes in the column as a function of the distance from the column

inlet; the amount of molecules involved in a 2-mm slice of the column contents (extruded from the column) is represented by a portion of the histogram (with a width of 2 mm). This has been estimated by using the method in Section (A), taking into account the fact that both turkey and chicken lysozymes have virtually the same ultraviolet adsorption coefficient. It can be seen in Fig. 1 that the distribution is almost rectangular in shape, with a total width of 16 mm.

Two curves obtained by connecting filled and unfilled circles in Fig. 1 represent the contributions of turkey and chicken lysozymes to the total histogram as estimated by chromatographing molecules contained in each portion of the histogram on an HA column, respectively. This is feasible since both types of lysozyme can almost completely be separated from each other on the HA column under small load conditions (cf. Fig. 6k), and the amount of molecules contained in a chromatographic peak can be estimated by measuring the area occupied by the peak.

The points in Fig. 2 are plots of the width of the initial molecular band versus total sample load for turkey and chicken lysozymes, and the 1:1 mixture of them. It can be seen in Fig. 2 that the relationship between band width and sample load is virtually independent of the type of the molecule, and that band width, in general, increases linearly with an increase in sample load. The straight line in Fig. 2 represents the regression line (passing through the origin) of band width on sample load.

(D) Preliminary Experiments under Conditions of Small Sample Loads

The first purpose of this subsection is to determine the function $f^{\circ}[m;\mu(s),\sigma(s;g)]$ (Eq. 16) or the function $G_{s,g}[m,\mu,\sigma(\mu)]$ (Eq. 19). For this purpose it is sufficient to evaluate the parameters φ, x', and Θ_0 that are involved in Eq. (16) or both Eqs. (17) and (18). When once the parameters φ, x', and Θ_0 are evaluated, q and μ can be considered to be functions of each other (see Eq. 17), and $G_{s,g}$ can finally be represented as a function of both m and q or both m and μ. [The method of the evaluation of the parameters φ, x', and Θ_0 is similar to that applied in an earlier paper (*14*) for the case of the column packed with plate-like HA crystals. In order to facilitate the understanding of the work in this subsection, the reader is recommended to first see Ref. *14*.] The second purpose consists in evaluating the parameters q (cf. Eqs. 17 and 18 or $q_{(\rho')}$ (cf. Eqs. 9 and 12) for both turkey and chicken lysozymes. This will be performed at the same time with the evaluation of the parameters x', φ, and Θ_0.

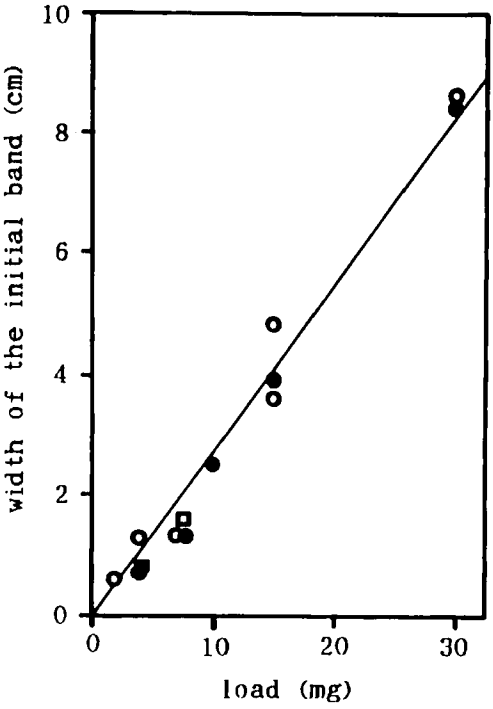

FIG. 2. The points are plots of the width of the initial molecular band versus total sample load for turkey (●) and chicken (○) lysozymes, and the 1:1 mixture (□) of them. The straight line is the regression line (passing through the origin) of band width on sample load.

Figures 3(a) and 3(b), respectively, represent $m_{elu(P)}$ and $\sigma_{(P)}$ for the chicken lysozyme chromatographic peak as functions of flow rate when L = 13 cm, $g'_{(P)}$ = 6.94 mM/mL [$g'_{(P)}(\phi = 1\text{ cm})$ = 2.5 mM/mL], $m_{in(P)}$ = 1 mM, and sample load = 30 μg. [By using the regression line in Fig. 2, it can be estimated that the width of the initial molecular band occurring when the sample load is 30 μg is only 0.08 mm, being virtually infinitesimal in comparison with the total column length (13 cm).] It can be seen in Fig. 3(a) that $m_{elu(P)}$ is virtually independent of flow rate, being consistent with the first principle of chromatography (Ref. *4*, Appendix III). All the experiments below will be performed by using a flow rate of 0.5 mL/min.

The points in Fig. 4(a) are experimental plots of $m_{elu(P)}$ for turkey lysozyme versus L for two different $g'_{(P)}$ [or $g'_{(P)}$ (ϕ = 1 cm)] values: 6.94 (or

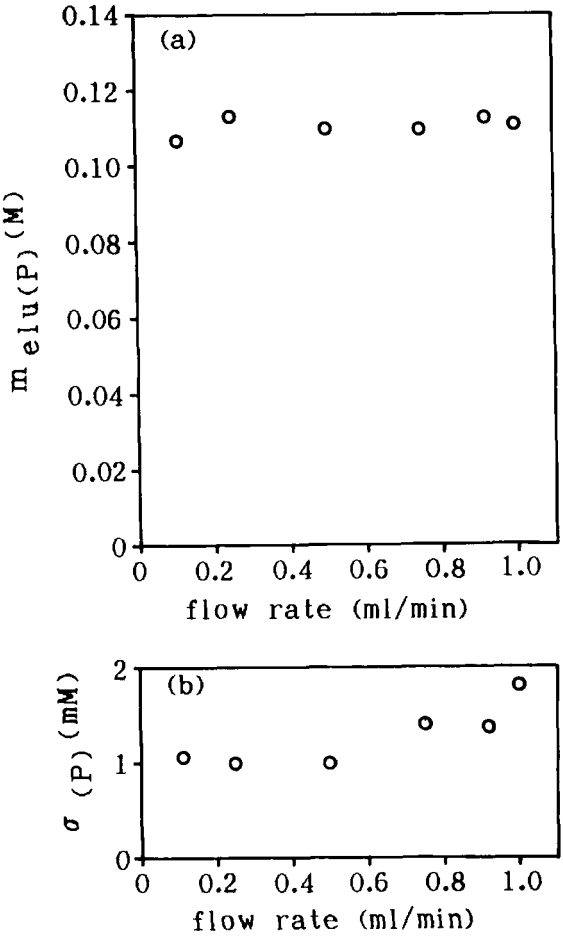

FIG. 3. (a) $m_{elu(P)}$ and (b) $\sigma_{(P)}$ for chicken egg white lysozyme as functions of flow rate as obtained when $L = 3 + 10 = 13$ cm, $g'_{(P)} = 6.94$ mM/mL [$g'_{(P)}(\phi = 1\text{ cm}) = 2.5$ mM/mL], and sample load = 30 μg. Other experimental conditions are: $m_{in(P)} = 1$ mM, $P = 0.9$–4.5 MPa, $T = 22.2$–25.5°C.

2.5) and 3.47 (or 1.25) mM/mL; the corresponding sample loads are 15–25 and 15–40 μg, respectively. It can be seen in Fig. 4(a) that the dependence of $m_{elu(P)}$ upon L differs when the $g'_{(P)}$ applied is different, giving two arrangements of the experimental points.

The points in Fig. 4(b) are plots of $m_{elu(P)}$ versus ln $s_{app(P)}$ instead of L for the experimental points in Fig. 4(a). It can be seen in Fig. 4(b) that the two arrangements of the experimental points in Fig. 4(a) converge into a single arrangement.

The points in Fig. 4(c) are experimental plots of $\sigma_{(P)}$ versus L for the points for $g'_{(P)}$ = 6.94 mM/mL in both Figs. 4(a) and 4(b).

The points in Figs. 5(a)–(c) are experimental plots for chicken lysozyme that correspond to those shown in Figs. 4(a)–(c) for turkey lysozyme, respectively. In Figs. 5(a)–(c), however, the experiment has been carried out over a wider range of the column length, and in Figs. 5(a) and 5(b), four different $g'_{(P)}$ [or $g'_{(P)}$ (ϕ = 1 cm)] values: 13.9 (or 5.0), 6.94 (or 2.5), 3.47 (or 1.25), and 1.25 (or 0.45) mM/mL have been applied; the corresponding sample loads are 16–30, 20–60, 30, and 50 μg, respectively. The points in Fig. 5(c) only correspond to the points for $g'_{(P)}$ = 6.94 mM/mL in both Figs. 5(a) and 5(b), however.

The curves in both Figs. 4(b) and 5(b) are theoretical, calculated by using Eq. (17) in which the term qs has been replaced by $q_{app}s_{app(P)}$ by using both Eqs. (23) and (24). In Eq. (17), the parameter m_{in} has a value of 1.5 mM since $m_{in(P)}$ = 1 mM, and the parameter φ (which characterizes competing potassium ions) has been assumed to be in the range of 10 to 50 M^{-1} on the basis of chromatographic experiments carried out by using several basic proteins including both turkey and chicken egg white lysozymes (*20*). If φ = 10 M^{-1}, best fits with the experiment can be obtained when $x' \approx 8$ and ln $q_{app} \approx 8.4$, and when $x' \approx 8$ and ln$q_{app} \approx 7.9$ for turkey and chicken lysozyme, respectively. If φ = 50 M^{-1}, best fits can be obtained when $x' \approx 5$ and ln $q_{app} \approx 11.9$, and when $x' \approx 5$ and ln $q_{app} \approx 11.4$ for turkey and chicken lysozyme, respectively. The theoretical curves in both Figs. 4(b) and 5(b) represent those that have finally been calculated by using an intermediate value, 25 M^{-1}, for the parameter ϕ, where, in order to have best fits with the experiment, it has been asumed: x' = 5.7 and ln q_{app} = 10.1 [Fig. 4(b)], and x' = 5.7 and ln q_{app} = 9.5 [Fig. 5(b)].

The curves in Figs. 4(a) and 5(a) represent the theoretical curves in Figs. 4(b) and 5(b) mapped on the (L,$m_{elu(P)}$) plane, respectively.

The curves in both Figs. 4(c) and 5(c) are theoretical, calculated by using Eq. (18) where $\sigma(s;g)$ = 1.5 $\sigma_{(P)}$, and, for the parameters φ, x', and ln q_{app}, the same values as those used for the calculation of the theoretical curves in

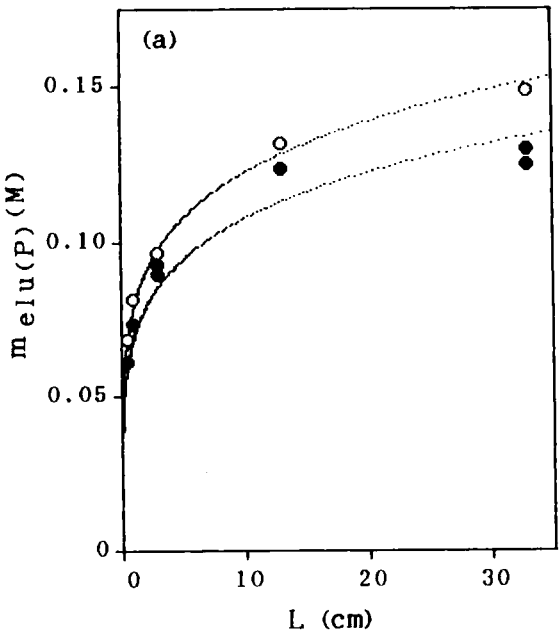

FIG. 4. Points: Experimental plots of (a) $m_{elu(P)}$ versus L, (b) $m_{elu(P)}$ versus ln $s_{app(P)}$, and (c) $\sigma_{(P)}$ versus L for turkey egg white lysozyme for two different $g'_{(P)}$ [or $g'_{(P)}(\phi = 1$ cm)] values: 6.94 (or 2.5) mM/mL (○) and 3.47 (or 1.25) mM/mL (●); the corresponding sample loads are 15–25 and 15–40 μg, respectively. [In (c), only the data for $g'_{(P)} = 6.94$ mM/mL are shown.] The total column length, L, applied to the experiments are 0.5, 1, 13 (= 3 + 10) and 33 (= 3 + 30) cm. Other experimental conditions are: $m_{in(P)} = 1$ mM, flow rate = 0.5 mL/min, P = 0.6–4.2 MPa, T = 22.2–26.2°C. Curves in (a) and (b): theoretical curves calculated by using Eq. (17) (in which the term qs is replaced by $q_{app}s_{app(P)}$ by using both Eqs. 23 and 24), where $m_{in} = 1.5$ mM, $\varphi = 25\ M^{-1}$, $x' = 5.7$, and ln $q_{app} = 10.1$. Curve in (c): Theoretical curve calculated by using Eq. (18) where $\Theta_0 = 0.005$ cm; for the parameters m_{in}, φ, x', and ln q_{app}, the same values as those used for the calculation of the theoretical curves in both (a) and (b) have been used, and the parameter q has been evaluated from the parameter q_{app} by using Eq. (24).

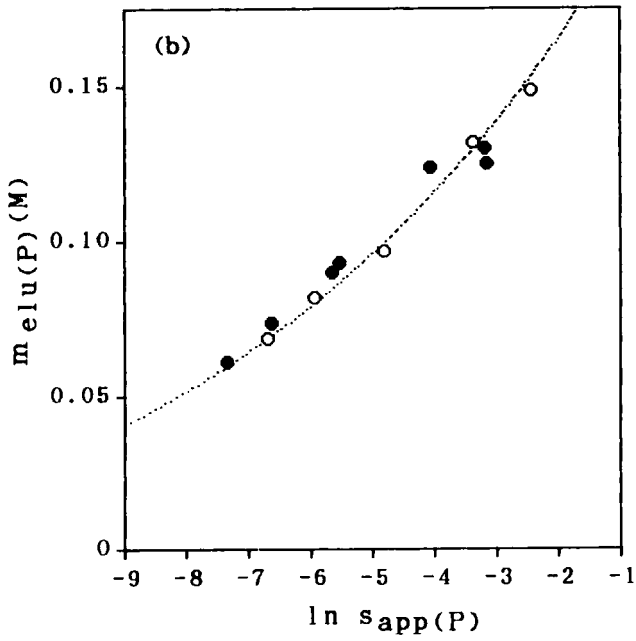

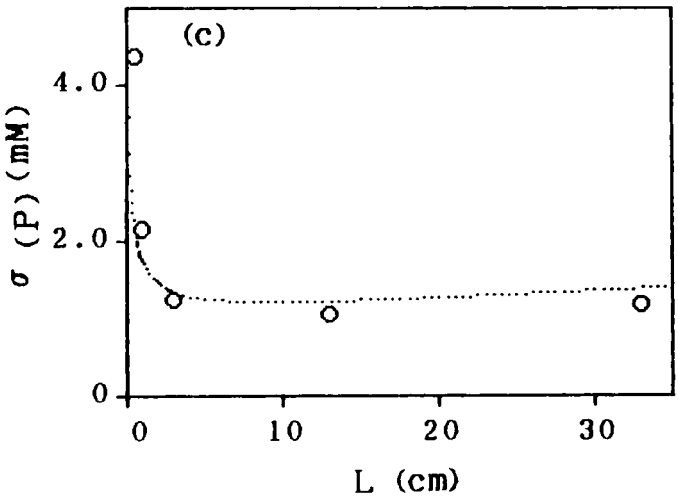

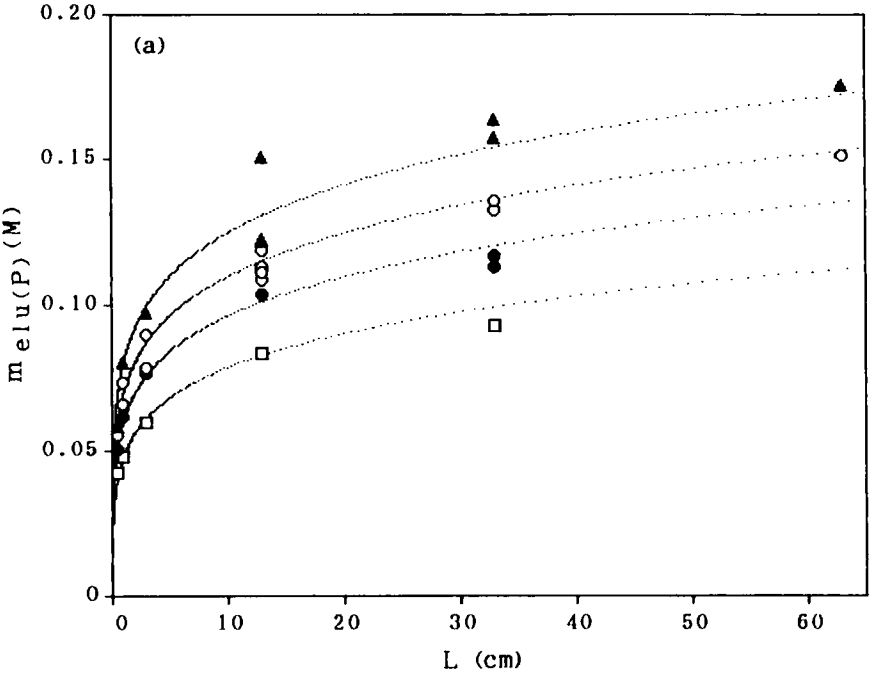

FIG. 5. Points: As in Fig. 4 for chicken egg white lysozyme. The experiment was carried out over a wider range of the column length with addition of the total column length, L, of 63 (= 3 + 2 × 30) cm, and four different $g'_{(P)}$[or $g'_{(P)}(\phi = 1$ cm)] values: 13.9 (or 5.0) mM/mL (▲), 6.94 (or 2.5) mM/mL (○), 3.47 (or 1.25) mM/mL (●), and 1.25 (or 0.45) mM/mL (□) have been applied; the corresponding sample loads are 16–30, 20–60, 30, and 50 μg, respectively. [In (c), only the data for $g'_{(P)}$ = 6.94 mM/mL are shown.] Other experimental conditions that are different from those in Fig. 4 are: P = 0.3–10.0 MPa, T = 21.0–29.7°C. Curves: As in Fig. 4, but it is assumed: ln q_{app} = 9.5.

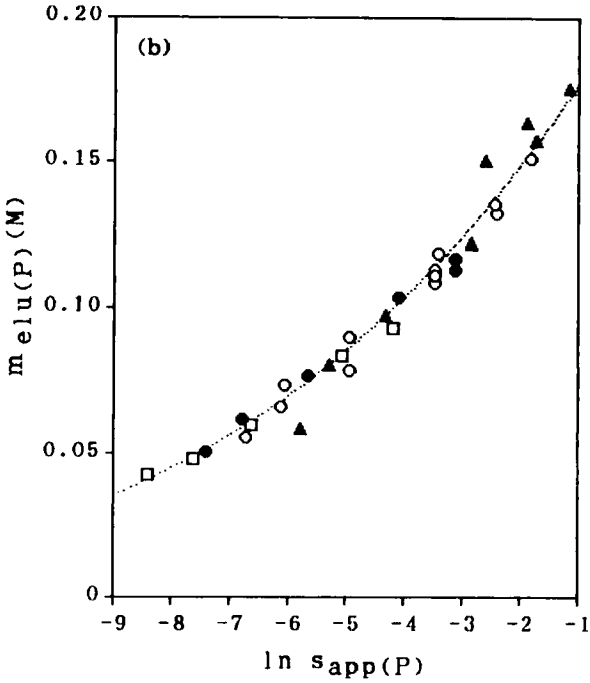

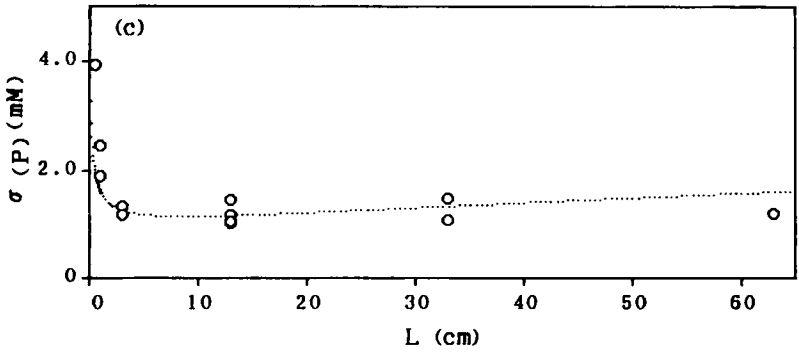

Figs. 4(a), 4(b), 5(a), and 5(b) have been used; the parameters ln q for turkey and chicken lysozyme have been evaluated to be 10.1 and 9.5 from the ln q_{app} values by using Eq. (24), respectively. As far as the parameter Θ_0 is concerned, a value of 0.005 cm has been obtained in both Figs. 4(c) and 5(c) in order to have best fits with the experiment.

In summary, best values of 25 M^{-1}, 5.7 and 0.005 cm, have been obtained for the experimental parameters φ, x', and Θ_0, respectively. At the same time, the parameters ln q or ln $q_{(\rho')}$ for turkey and chicken lysozyme have been evaluated to be 10.1 and 9.5, respectively. These values will hereafter be used for all the calculations.

(E) Experiments under Overload Conditions

Figure 6 illustrates experimental chromatograms of turkey lysozyme [(a)-(e)], chicken lysozyme [(f)-(j)] and 1:1 mixtures of both types of lysozyme [(k)-(n)] obtained for different sample loads when L = 13 cm, $g'_{(P)}$ = 6.94 mM/mL [$g'_{(P)}(\varphi$ = 1 cm) = 2.5 mM/mL] and $m_{in(P)}$ = 1 mM. Filled and unfilled circles in Fig. 6(n) represent the contributions of turkey and chicken lysozyme to the total chromatogram as estimated on the basis of the rechromatography experiment, respectively. It can be seen in Fig. 6 that the position (or the phosphate molarity) at which a chromatogram begins migrates toward the left (or the low phosphate molarity) as the sample load increases; the width of the chromatogram increases, and the total shape of the chromatogram tends to be a shape close to a right-angled triangle with tailing at the same time. [It can also be seen in Fig. 6 that, under small sample load conditions (Parts (a), (f) and (k)), the Buffer A molarity gradient increases linearly with a lapse of time. Under overload conditions (the other parts of Fig. 6), however, the gradient is disturbed due to the presence of the chromatographic peak. This phenomenon can be considered to be apparent, mainly arising from the fact that the refractive index of the solution is disturbed; this is provoked by a quick change of the concentration of the sample molecules in the flow cell. For the monitoring method of the molarity gradient, see Section (A).]

Figures 7(a)-(n) illustrate theoretical chromatograms that correspond to the experimental chromatograms shown in Fig. 6, calculated on the basis of the quasi-crystalline phase model using Eqs. (5)-(7), (10)-(12), and (14)-(20). For the calculation, both parameters s and $\chi^*_{(\rho')}$ have been evaluated for each sample load by using the regression line in Fig. 2; for the parameters φ, x', Θ_0, $q_{(1)}$, and $q_{(2)}$ (where the suffixes 1 and 2 stand for turkey and chicken lysozyme, respectively), the values obtained in Section

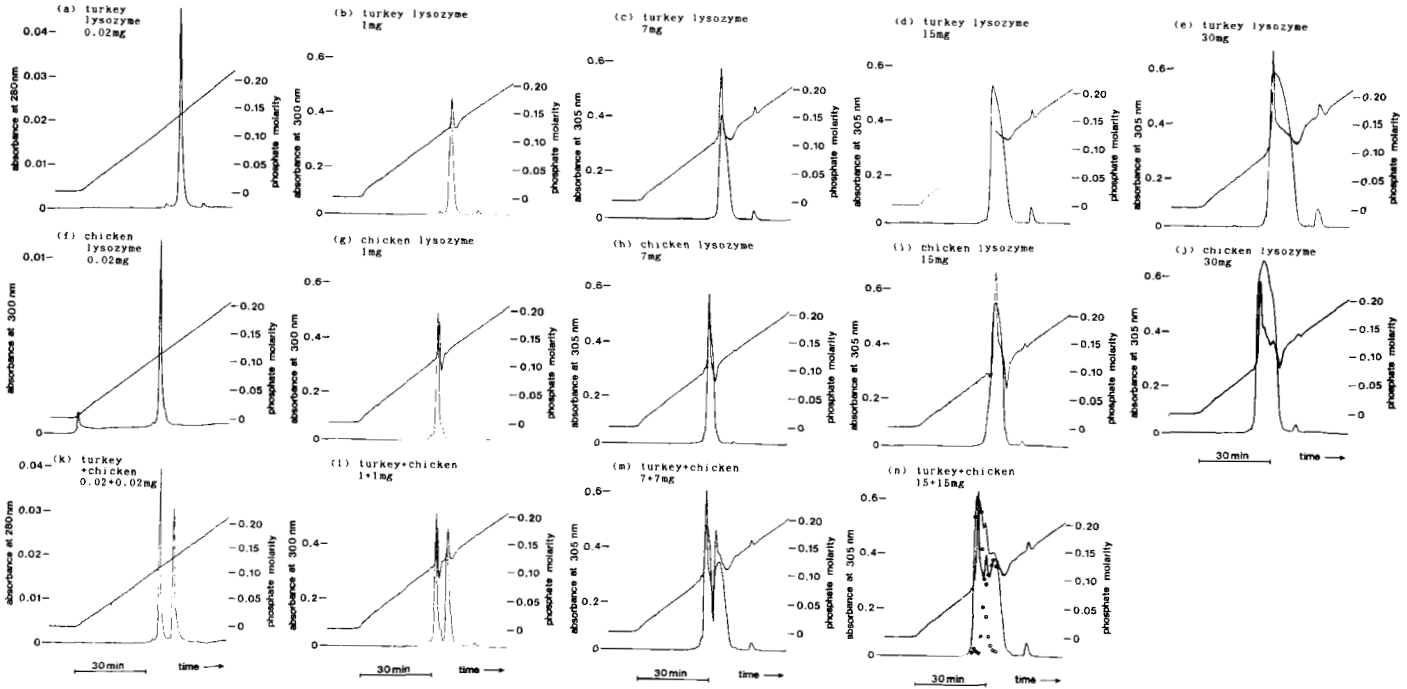

FIG. 6. Experimental chromatograms of turkey egg white lysozyme [with loads of 0.02, 1, 7, 15, and 30 mg; (a)–(e)], chicken egg white lysozyme [with loads of 0.02, 1, 7, 15, and 30 mg; (f)–(j)], and 1:1 mixtures of both types of lysozyme [with loads of 0.02, 1, 7, and 15 mg for each component; (k)–(n)] as obtained on a HA column when $L = 3 + 10 = 13$ cm, $g'_{(P)} = 6.94$ mM/mL [$g'_{(P)}(\phi = 1\text{ cm}) = 2.5$ mM/mL] and $m_{in(P)} = 1$ mM. Other experimental conditions are: flow rate = 0.5 mL/min, $P = 1.6$–2.5 MPa, $T = 23.5$–26.5°C. Filled and unfilled circles in Part (n) represent the contributions of turkey and chicken lysozymes to the total chromatogram as estimated on the basis of the rechromatography experiment, respectively.

(D) have been used. As far as the parameter $\hat{E}$ (Eq. 11) is concerned, the values of 0.4 kcal/mol and 0.2 kcal/mol at 25°C have been used for the turkey and the chicken lysozyme systems [Figs. 7(a)–(e) and Figs 7(f)–(j)] in order to have best fits with the experiment, respectively (cf. Fig. 8); for the 1:1 mixtures of the two types of lysozyme, the average value, 0.3 kcal/mol has been assumed [Figs. 7(k)–(n)]. It can be seen in Fig. 7 that the potassium or the phosphate molarity at which a chromatogram begins migrates toward the low molarity as the sample load increases; the width of the chromatogram increases, and the total shape of the chromatogram tends to be a shape close to a right-angled triangle with tailing at the same time in parallel with the experiment (Fig. 6). [When too large an amount of molecules is loaded on the column, however, the shape of the theoretical chromatogram deviates from that of the experimental one. For instance, cf. Figs 7(e) and 7(j) with Figs. 6(e) and 6(j), respectively. Also see Fig. 8(b) and the Discussion Section.]

Figures 7(d′), 7(i′), and 7(n′) illustrate theoretical chromatograms that correspond to those in Figs. 7(d), 7(i), and 7(n), or those in Figs. 6(d), 6(i), and 6(n) obtained on the basis of the amorphous phase model using Eqs. (5)–(7), (10)–(13), and (15)–(20), respectively; for the parameters involved in the equations, the same values as those used for the calculation for Figs. 7(d), 7(i), and 7(n) have been assumed. It can be seen in Figs. 7(d′), 7(i′), and 7(n′) that the total shapes of the chromatograms are close to a rectangle rather than a right-angled triangle, in disaccordance with the experiment (Fig. 6).

The points in Fig. 8 are experimental plots of (a) $m_{elu(P)}$ and (b) $\sigma_{(P)}$ for turkey and chicken lysozymes (represented by filled and unfilled circles, respectively) versus sample load obtained when the two types of molecule are loaded independently on the column; the $m_{elu(P)}$ value has been estimated by interpolating the undisturbed parts of the molarity gradient if the gradient is apparently disturbed (cf. Fig. 6). The experimental conditions used in Fig. 8 are similar to those applied in Fig. 6, and most of the experimental points in Fig. 8 correspond to the experimental chromatograms in Figs. 6(a)–(j). The continuous and the dotted curves in Fig. 8 are theoretical, calculated on the basis of the quasi-crystalline phase model for turkey and chicken lysozyme, respectively; for the parameter $\hat{E}$, three values of 0.3, 0.4, and 0.5 kcal/mol at 25°C have been assumed for turkey lysozyme, and three values of 0.1, 0.2, and 0.3 kcal/mol at 25°C for chicken lysozyme. It can be seen in Fig. 8(a) that, for the behavior of $m_{elu(P)}$, good fits between the theory and the experiment are obtained when $\hat{E}$ = 0.4 kcal/mol and $\hat{E}$ = 0.2 kcal/mol for turkey and chicken lysozyme, respectively. As far as the behavior of $\sigma_{(P)}$ is concerned, however, approximate

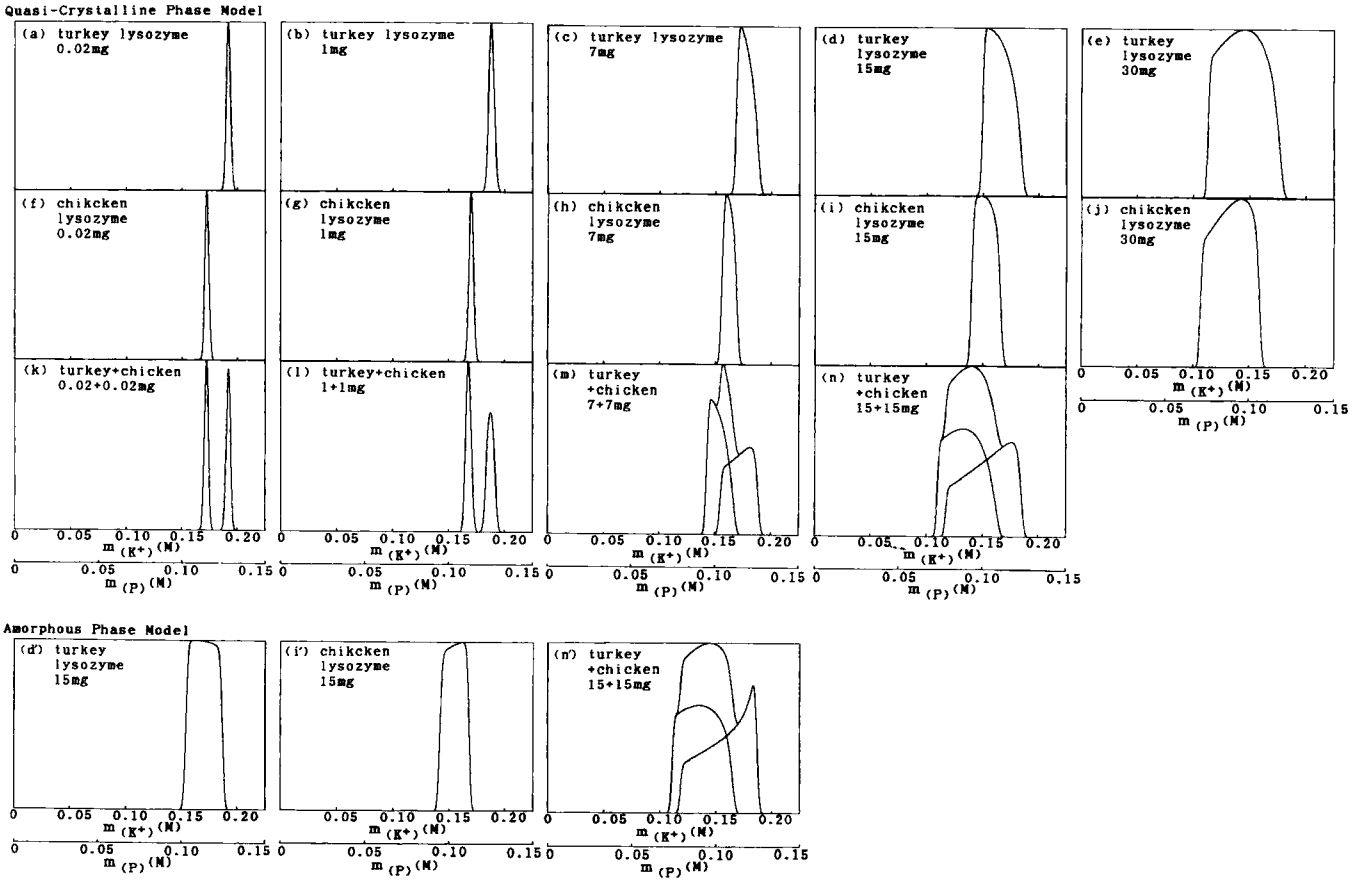

FIG. 7. Parts (a)–(n) represent theoretical chromatograms that correspond to the experimental chromatograms shown in Fig. 6, calculated on the basis of the quasicrystalline phase model using Eqs. (5)–(7), (10)–(12), and (14)–(20). Parts (d'), (i'), and (n') represent theoretical chromatograms that correspond to those in Parts (d), (i), and (n), or those in Figs. 6(d), (i), and (n) obtained on the basis of the amorphous phase model using Eqs. (5)–(7), (10)–(13), and (15)–(20). For details, see text.

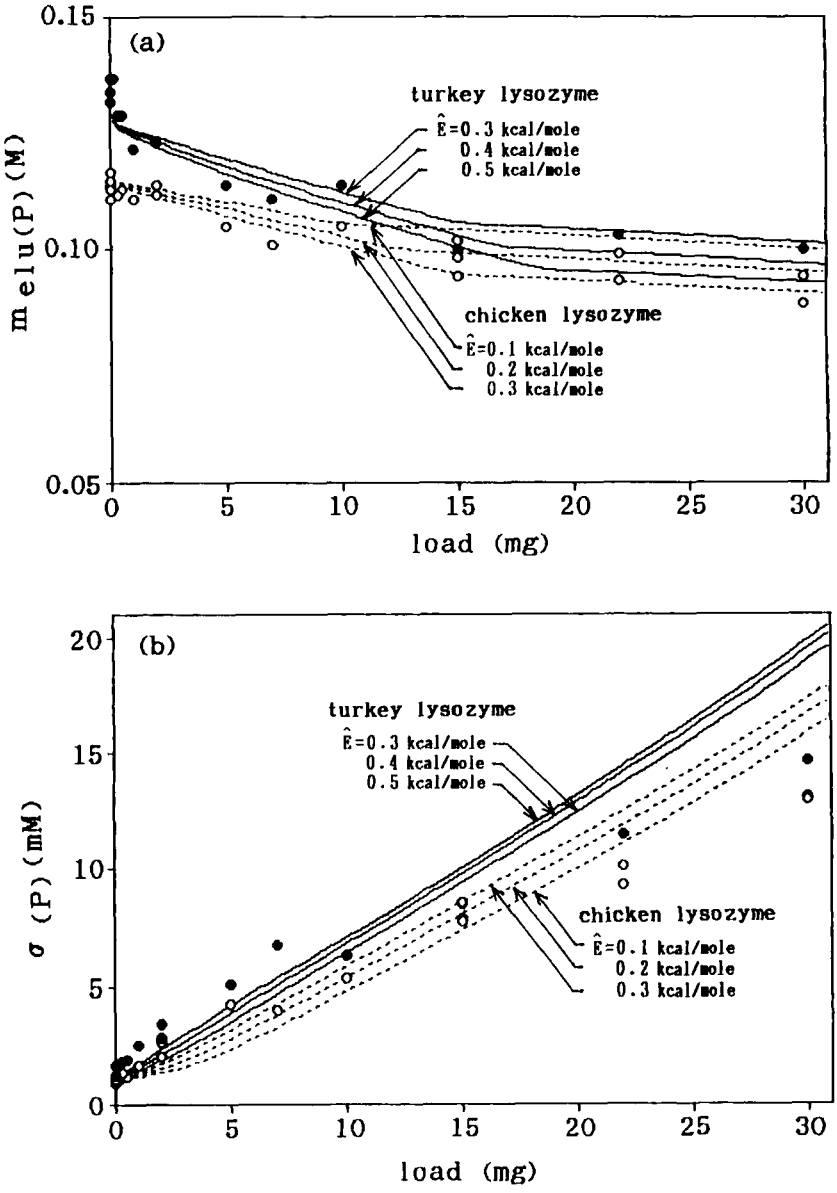

FIG. 8. Points: Experimental plots of (a) $m_{elu(P)}$ and (b) $\sigma_{(P)}$ for turkey (●) and chicken (○) egg white lysozymes versus sample load obtained when the two types of lysozyme are loaded independently on the column. Experimental conditions are: L = 3 + 10 = 13 cm, $g'_{(P)}$ = 6.94 mM/mL [$g'_{(P)}(\Phi$ = 1 cm) = 2.5 mM/mL], $m_{in(P)}$ = 1 mM, flow rate = 0.5 mL/min, P = 1.6–2.5 MPa, T = 20.0–29.0°C. Continuous curves: Theoretical curves calculated on the basis of the quasi-crystalline phase model for turkey egg white lysozyme assuming $\hat{E}$ = 0.3, 0.4, and 0.5 kcal/mol at 25.0°C. Dashed curves: Theoretical curves calculated on the basis of the quasi-crystalline phase model for chicken egg white lysozyme assuming $\hat{E}$ = 0.1, 0.2, and 0.3 kcal/mol at 25.0°C. For details, see text.

fits between the theory and the experiment can be obtained only when the sample load is small enough (i.e., when it is less than about 15 mg); when too large an amount of molecules is loaded on the column, the theoretical curves deviate from the experimental plots [see Fig. 8(b)]. This problem will be argued in the Discussion Section.

DISCUSSION

By introducing the quasi-crystalline phase model, theoretical chromatograms with shapes close to those of experimental chromatograms have been obtained when $\hat{E} = 0.2$–0.4 kcal/mol [Figs. 7(a)–(n)]. It has also been confirmed that the change in shape of the theoretical chromatogram with a change in sample load occurs in parallel with the experiment [cf. Figs. 7(a)–(n) with Fig. 6]. These verify the theory of overload quasi-static linear gradient chromatography [Theoretical Section], and it can be deduced that a quasi-crystalline phase of lysozyme molecules, in fact, is realized on the HA surfaces in the column.

It should be emphasized, however, that the quasi-crystalline phase model itself only represents the approximate feature of the molecules adsorbed on the adsorbent surface, provided Assumptions (a)–(e) in Appendix I hold good. It is therefore necessary to be very careful when interpreting the experimental result in terms of the model. For instance, in contrast to Assumption (d) in Appendix I, it would actually be possible that both the shape of an elementary domain and the relative geometrical relationship among the elementary domains vary with a change in total molecular density, χ, on the adsorbent surface. Provided the variation proceeds slowly enough, however, Assumption (d) in Appendix I would hold approximately. It can be suggested that the discrepancy between the theory and the experiment ocurring when too large an amount of molecules is loaded on the column [for instance, cf. Figs. 7(e) and 7(j) with Figs. 6(e) and 6(j), respectively] arises at least partially from the fact that the shape of an elementary domain and/or the relative geometrical relationship among the elementary domains actually change(s) slightly with an increase in total molecular density, χ, on the adsorbent surface.

The last half of Assumption (e) in Appendix I states that the probability that two molecules keep in contact with each other on the adsorbent surface is proportional to the molecular density occurring in the direction perpendicular to the active surface of a given molecule which is able to keep in contact with the surfaces of other molecules. It should be noted that this assumption is true provided the location of a given molecule oc-

curs at random in the direction under consideration on the adsorbent surface (Bragg-Williams approximation). Due to repulsive molecular interactions, however, the probability of the occurrence of the mean arrangement of the molecules on the adsorbent surface should be much higher than the probability that other arrangements occur. [This deduction is adopted as Assumption (b) in Appendix I.] In other words, the probability that two molecules are separated to a certain extent should be much higher than the probability that they approach closely to each other. This means that the last half of Assumption (e) in Appendix I (see above) holds only approximately. Further, in connection with the argument above, it can be deduced that the $\hat{E}$ value of 0.2–0.4 kcal/mol that has been estimated on the basis of Assumption (e) in Appendix I is apparent, and that it is (much) smaller than the actual value of the interaction energy per molecule occurring provided the maximum possible contact with other molecules is made on the adsorbent surface. If the phases of two neighboring rows of elementary domains are staggered [as represented by Parts (a′)-(c′) and (c″) of Fig. A1 in Appendix I], the apparent $\hat{E}$ value would still be small in comparison with the actual value since, in this instance, the molecular density occurring in the direction perpendicular to the active surface of a given molecule is proportional to $\sqrt{\chi}$ with a proportionality constant smaller than unity except when χ is close to unity [cf. the explanation in brackets of Assumption (e) in Appendix I]. The deduction that the apparent $\hat{E}$ value of 0.2–0.4 kcal/mol is (much) smaller than the actual value is reasonable since it would be necessary that the $\hat{E}$ value be (much) larger than the order of the kT value or 0.6 kcal/mol at 25°C in order for the quasi-crystalline phase to be preferentially realized to the amorphous phase.

Earlier (*21*), tacitly applying the quasi-crystalline phase model [characterized by Assumptions (a)-(e) in Appendix I], the apparent $\hat{E}$ value of 3 kcal/mol was obtained for the collagen molecule. Since a collagen molecule can be represented by a rod of dimensions 15 × 3000 Å (*22*) in contrast to a lysozyme molecule which can be represented by a prolate spheroid of dimensions 45 × 30 × 30 Å (*12*), the $\hat{E}$ value for collagen seems to be compatible with the corresponding value for lysozyme (0.2–0.4 kcal/mol). For the estimation of the $\hat{E}$ value for collagen, a further assumption is involved concerning the property of the assembly of the molecules, however (see Ref. *21*).

APPENDIX I : SPECIFICATION OF THE QUASI-CRYSTALLINE PHASE MODEL (*11*)

With regard to the quasi-crystalline phase model originally introduced in an earlier paper (*11*) (cf. the Introduction Section), an additional explanation is given below. Thus, in Fig. A1 the squares with a bold outline (each of which represents a molecule) schematically depict several types of the mean geometrical arrangement of the molecules on the adsorbent surface, constituting several types of the quasi-crystalline phase. The illustration in Fig. A1 is made for the case when all the molecules have the same dimensions and the same shape, and, as far as molecules with any asymmetrical shape are concerned, the main axis of any molecule is orienting in the abscissa direction; the abscissa scale of the diagram is reduced in order that a molecule appears as if it were symmetrical in shape (as schematically represented by a square). Therefore, the molecular interaction occurs mainly through side faces of the molecules that are parallel to one another.

The quasi-crystalline phase of the molecules as generating (Eq. 14) would be realized if the following assumptions are fulfilled:

(a) The molecular densities in the abscissa and the ordinate direction on the adsorbent surface are virtually equal to each other on average. Here, the molecular density means the proportion of the part of the adsorbent surface that is occupied by the molecules.

(b) Given the total molecular density, χ, on the adsorbent surface, the probability of the occurrence of the *mean* arrangement of the molecules [as represented by Fig. A1; cf. Assumption (c)] is much higher than the probability that other molecular arrangements occur.

(c) The mean molecular arrangement on the adsorbent surface is made in such a way that the total adsorbent surface can be divided into equal elementary domains in each of which a single molecule is involved.

(d) Both the shape of an elementary domain and the relative geometrical relationship among the elementary domains [cf. Assumption (c)] are similar if the total molecular density, χ, on the adsorbent surface changes. [Parts (a)–(c) of Fig. A1 represent the case when the phases between any rows of elementary domains occurring in the abscissa direction are equal to one another, independent of the total molecular density, χ, on the ad-

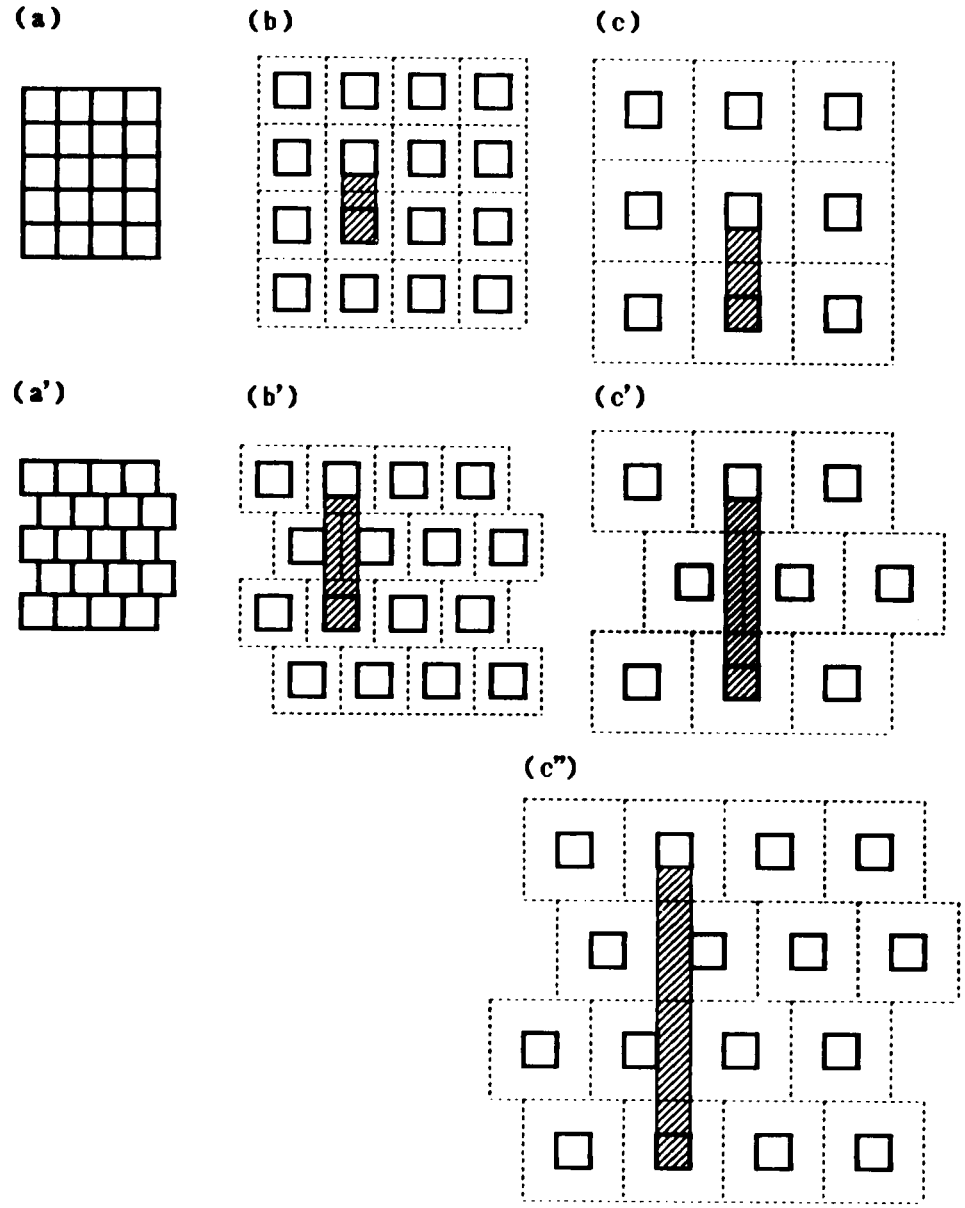

FIG. A1. Schematical representation of the quasi-crystalline phase model. For details, see text.

sorbent surface, decreasing in the order of (a)→(b)→(c). Parts (a′)–(c′) represent the case when the phases of two neighboring rows of elementary domains are staggered by a factor of 1/2 the size of an elementary domain; Part (c″) is the case when the stagger occurs by a factor of 1/3 the size of an elementary domain.]

(e) The energetic molecular interaction occurs only when two molecules keep in contact with each other, and the probability that two molecules keep in contact with each other on the adsorbent surface (being proportional to the interaction energy *on average with respect to time* per molecule) is proportional to the molecular density occurring in the direction perpendicular to the active surface of a *given* molecule which is able to keep in contact with surfaces of other molecules. [In Fig. A1 the height of a shadowed rectangle is inversely proportional to the molecular density occurring in the direction perpendicular to the active surface of the given molecule that is parallel to the abscissa direction; with molecules with an asymmetrical shape, the active surface corresponds to side faces of the molecules that are parallel to one another. If the phases between any rows of elementary domains are always equal to one another, as is the case with Parts (a)–(c) of Fig. A1 (cf. Assumption (d)), then the molecular density occurring in the direction perpendicular to the active surface of the given molecule is proportional to $\sqrt{\chi}$ with a proportionality constant equal to unity. If the phases of two neighboring rows of elementary domains are staggered, then the corresponding molecular density is proportional to $\sqrt{\chi}$ with a proportionality constant smaller than unity. In fact, under the situation represented by Parts (b′) and (c′) of Fig. A1, the proportionality constant is equal to 1/2. In this latter case, however, the molecular density under consideration is exceptionally disproportional to $\sqrt{\chi}$ when χ tends to its maximum value of unity; see Part (a′) of Fig. A1.]

Both Assumptions (d) and (e) are argued in detail in the Discussion Section. The arguments above that have been made on the basis of the illustration in Fig. A1 can be extended to cases where the molecules are heterogeneous in both dimensions and shape if further assumptions are added.

APPENDIX II: RELATIONSHIP WITH THE EARLIER THEORY (*11*)

The asymptotic expression of the theoretical chromatogram (Eqs. 6 and 7) occurring provided

$$x' \approx \infty \qquad \text{(A1)}$$

$$E_{(\rho')} + kT \ln t_{(\rho')} = O(x') \tag{A2}$$

and

$$\hat{E} = O(x') \tag{A3}$$

(cf. Eqs. 5–7 in Ref. *11*) in the absence of longitudinal diffusion in the column has been derived in an earlier paper (*11*). The asymptotic chromatogram is independent of s or $\hat{s}$, and it can be represented by Eq. (54) in Ref. *11* as

$$\hat{f}_{(\rho')}(m) = 0 \left(m_{in} < m < \frac{e^{[\eta_{(\rho')} - \hat{\eta}\zeta(\Sigma_{\rho''=1}^{\rho'} \chi^*_{(\rho'')})]/kT} - 1}{\varphi} \right) \tag{A4a}$$

$$\hat{f}_{(\rho')}(m) = -\frac{d}{dm} \zeta^{-1} \left[\frac{\eta_{(\rho')} - kT \ln (\varphi m + 1)}{\hat{\eta}} \right]$$

$$\left(\frac{e^{[\eta_{(\rho')} - \hat{\eta}\zeta(\Sigma_{\rho''=1}^{\rho'} \chi^*_{(\rho'')})]/kT} - 1}{\varphi} < m < \right.$$

$$\left. \frac{e^{[\eta_{(\rho')} - \hat{\eta}\zeta(\Sigma_{\rho''=1}^{\rho'} \chi^*_{(\rho'')})]/kT} - 1}{\varphi} \right) \tag{A4b}$$

$$\hat{f}_{(\rho')}(m) = 0 \left(m > \frac{e^{[\eta_{(\rho')} - \hat{\eta}\zeta(\Sigma_{\rho''=1}^{\rho'} \chi^*_{(\rho'')})]/kT} - 1}{\varphi} \right) \tag{A4c}$$

in which ζ^{-1} represents the inverse function of ζ, and the sum $\Sigma_{\rho''=1}^{0} \chi^*_{(\rho'')}$ is defined to be zero; $\hat{\eta}$ and $\eta_{(\rho')}$ are defined to be

$$\hat{\eta} = \hat{E}/x' \tag{A5}$$

and

$$\eta_{(\rho')} = \frac{E_{(\rho')} + kT \ln \tau_{(\rho')} + kT \ln \beta}{x'} = \frac{kT \ln q_{(\rho')}}{x'} \tag{A6}*$$

(cf. Eq. 9), respectively. With the amorphous and the quasi-crystalline phase model fulfilling Eqs. (13) and (14), in Eq. (A4b) can be rewritten as

$$\hat{f}_{(\rho')}(m) = \frac{\varphi kT}{\hat{\eta}} \cdot \frac{1}{\varphi m + 1} \tag{A7}$$

and

$$\hat{f}_{(\rho')}(m) = \frac{2\varphi kT}{\hat{\eta}^2} \cdot \frac{\eta_{(\rho')} - kT \ln (\varphi m + 1)}{\varphi m + 1} \tag{A8}$$

respectively.

Equations (A4a)–(A4c) can approximately be represented as

$$\hat{f}_{(\rho')}(m) = 0 \left(m_{in} \leqslant m < \frac{\eta_{(\rho')} - \hat{\eta}\zeta\left(\sum_{\rho''=1}^{\rho'} \chi^*_{(\rho'')}\right)}{\varphi kT} \right) \tag{A9a}$$

$$\hat{f}_{(\rho')}(m) = -\frac{d}{dm} \zeta^{-1}\left[\frac{\eta_{(\rho')} - kT\varphi m}{\hat{\eta}} \right]$$

$$\left(\frac{\eta_{(\rho')} - \hat{\eta}\zeta\left(\sum_{\rho''=1}^{\rho'} \chi^*_{(\rho'')}\right)}{\varphi kT} \leqslant m < \right.$$

$$\left. \frac{\eta_{(\rho')} - \hat{\eta}\zeta\left(\sum_{\rho''=1}^{\rho'-1} \chi^*_{(\rho'')}\right)}{\varphi kT} \right) \tag{A9b}$$

*Due to both Eqs. (A1) and (A2), it is possible to define $\eta_{(\rho')}$ simply as $\eta_{(\rho')} = [E_{(\rho')} + kT \ln \tau_{(\rho')}]/x'$. This definition of $\eta_{(\rho')}$ is applied in Eq. (13) in Ref. *11*.

$$\hat{f}_{(\rho')}(m) = 0 \left(m > \frac{\eta_{(\rho')} - \hat{\eta}\zeta\left(\sum_{\rho^*=1}^{\rho'-1} \chi^*_{(\rho^*)}\right)}{\varphi kT}\right) \tag{A9c}$$

which are equivalent to Eq. (77) in Ref. *11* . With the amorphous and the quasi-crystalline phase model fulfilling Eqs. (13) and (14), Eq. (A9b) can be rewritten as

$$\hat{f}_{(\rho')}(m) = \frac{\varphi kT}{\hat{\eta}} \tag{A10}$$

and

$$\hat{f}_{(\rho')}(m) = \frac{2\varphi kT}{\hat{\eta}^2}(\eta_{(\rho')} - kT\varphi m) \tag{A11}$$

respectively.

Provided the amount of sample molecules involved in an elementary volume of the column is small (as is the case with chromatography under small load conditions), the partition, B', of sample molecules (of the chromatographic component under consideration) in the mobile phase in the elementary volume can be represented as a function of molarity, m, of competing ions by using Eq. (29) in Ref. *17*. This can be written as

$$B'(m) = \frac{1}{1 + q(\varphi m + 1)^{-x'}} = \frac{1}{1 + Z^{-x'}} \tag{A12}*$$

in which

$$Z = \frac{\varphi m + 1}{q^{1/x'}} \tag{A13}†$$

The continuous and the dotted curve indicated by $x' = 5.7$ in Fig. A2 represent the functions $B'(m_{(K^+)})$ for turkey and chicken egg white lysozyme

*Equation (A12) also appears as Eq. (44) in Ref. *4*.

†Z corresponds to $Y_{(\rho')}$ in Ref. *11*. In order to avoid the confusion with $Y_{(\rho')}(\chi_{(\rho')})$ in the present paper (see Eqs. 6, 7, and 10), however, we use the symbol Z instead of Y.

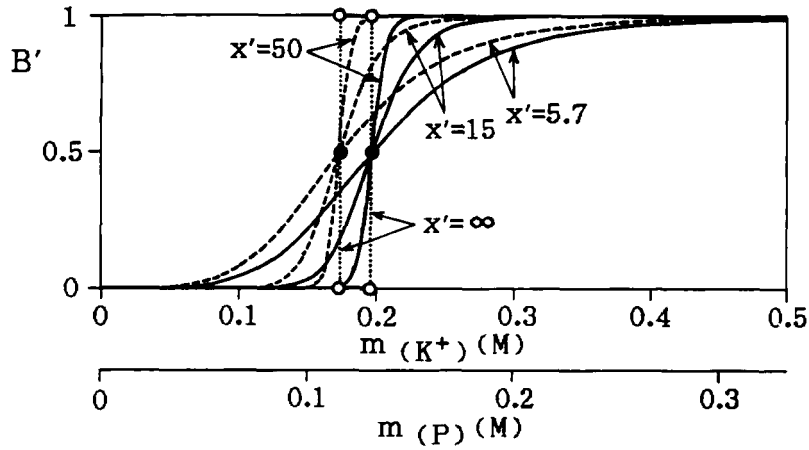

FIG. A2. The continuous and the dotted curves indicated by $x' = 5.7$ represent the functions $B'(m_{(K^+)})$ for turkey and chicken egg white lysozyme calculated by using Eq. (A12), respectively. The continuous and the dotted curves indicated by $x' = 15, x' = 50$, and $x' = \infty$ represent those that have been obtained by increasing the x' value while keeping the $q^{1/x'}$ or the $\eta \equiv (kT \ln q)/x'$ values equal to those for turkey and chicken lysozyme, respectively. On the abscissa, the $m_{(P)}$ value in Buffer A, which is 2/3 the $m_{(K^+)}$ value, is also shown. For details, see text.

calculated by using Eq. (A12), respectively; for the values of the experimental parameters, φ, x', and q involved in Eq. (A12), those that had finally been obtained in Experimental Section (D) have been applied. The continuous and the dotted curves indicated by $x' = 15, x' = 50$, and $x' = \infty$ in Fig. A2 represent those that have been obtained by increasing the x' value while keeping the $q^{1/x'}$ or the $\eta \equiv (kT \ln q)/x'$ (cf. Eq. A6) values equal to those for turkey and chicken lysozyme, respectively. When $x' = \infty$, B' is a step function of $m_{(K^+)}$ constituted of three parts: $B' = 0$ $[m_{(K^+)} < (q^{1/x'} - 1)/\varphi]$, $B' = 1/2$ $[m_{(K^+)} = (q^{1/x'} - 1)/\varphi]$, and $B' = 1$ $[m_{(K^+)} > (q^{1/x'} - 1)/\varphi]$.

Figures A3 and A4 illustrate theoretical chromatograms for model molecules characterized by the curves in Fig. A2, obtained under overload conditions in the absence of longitudinal diffusion in the column; Figs. A3 and A4 have been calculated by using the amorphous and the quasi-crystalline phase model, respectively. Thus, Parts (a)-(e) of both Figs. A3 and A4 represent single component chromatograms for molecules characterized by continuous curves indicated by $x' = 5.7, x' = 15, x' = 50$, and $x' = \infty$ in Fig. A2, and Parts (a')-(e') in both Figs. A3 and A4 represent

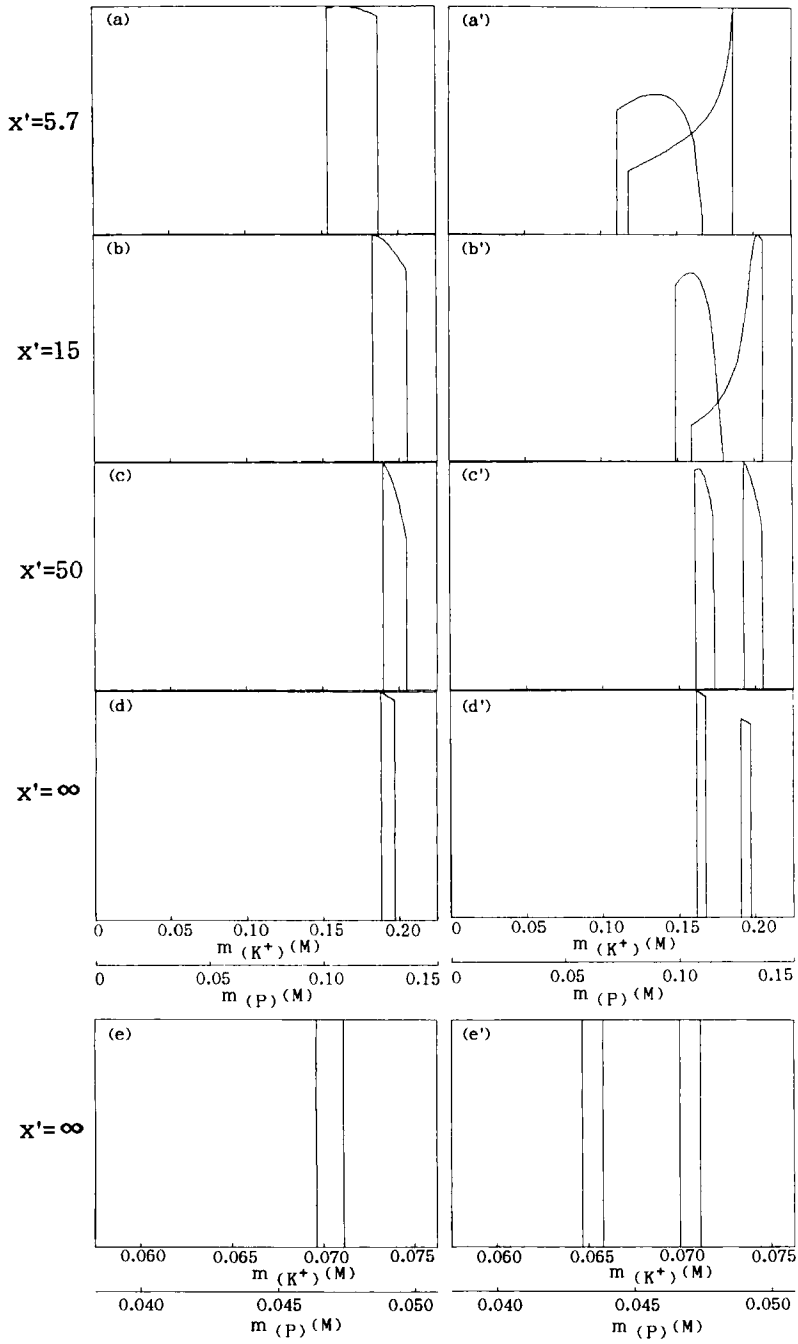

FIG. A3. Theoretical chromatograms for the model molecules characterized by the curves in Fig. A2, obtained under overload conditions in the absence of longitudinal diffusion in the column; this has been calculated by using the amorphous phase model. For details, see text.

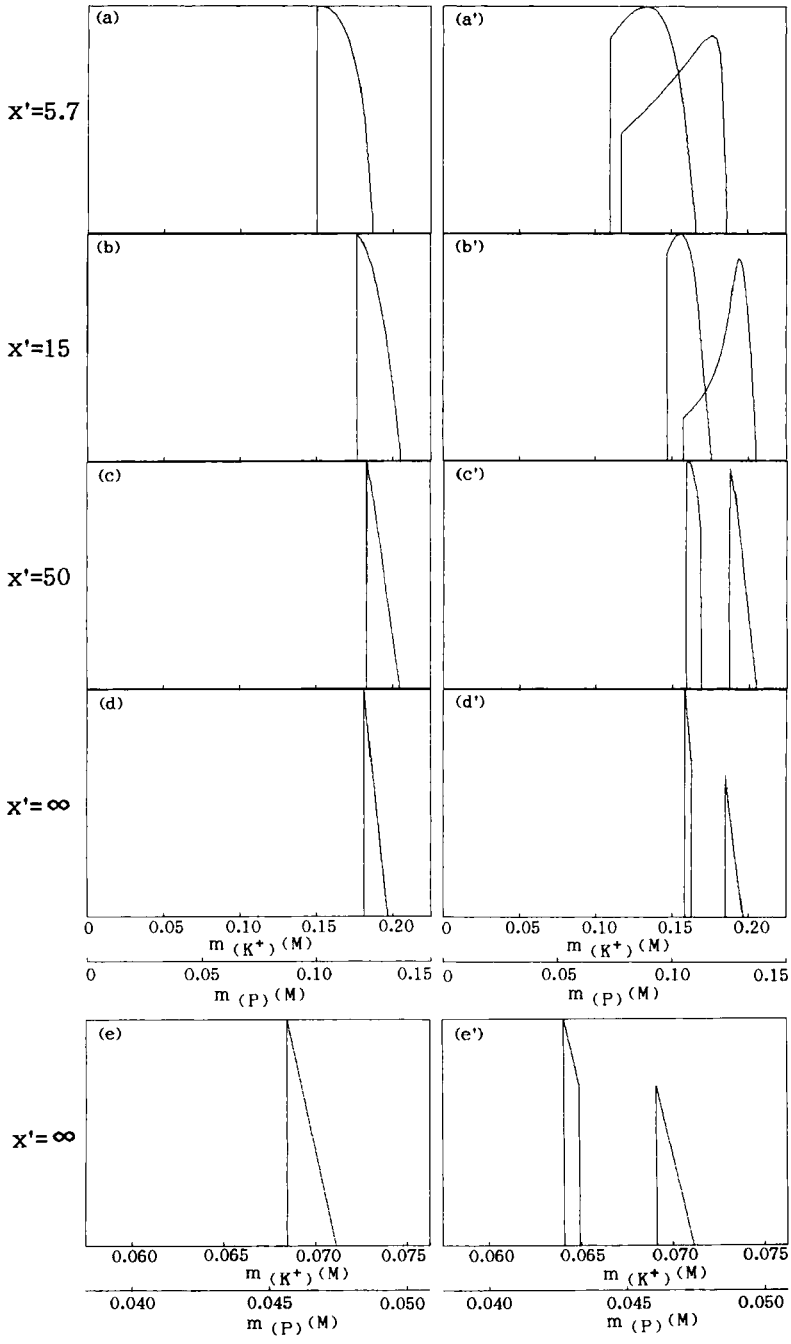

FIG. A4. As for Fig. A3 but calculated by using the quasi-crystalline phase model. For details, see text.

double component chromatograms for 1:1 mixtures of molecules with equal x' values of 5.7, 15, 50, and ∞; the two components of any mixture are characterized by continuous and dotted curves in Fig. A2, respectively. In both Figs. A3 and A4, Parts (a)-(c), (a')-(c') have been calculated by using both Eqs. (6) and (7) whereas Parts (d) and (d') and Parts (e) and (e') have been calculated by using Eqs. (A4a)-(A4c) and (A9a)-(A9c), respectively. Other assumptions for the calculation of the theoretical chromatograms in both Figs. A3 and A4 are as follows. Thus, in any part of the figures, the total amount, $\chi^*_{(\rho')}$ or $\Sigma^{\rho}_{\rho''=1}\chi^*_{(\rho'')}$, of molecules loaded on the column is equal to that assumed for the calculation of Figs. 7(d), 7(i), 7(n), 7(d'), 7(i'), and 7(n'). The $\hat{\eta}$ values (see Eq. A5) in Parts (a)-(e) and Parts (a')-(e') are equal to those assumed for the calculation of Figs. 7(d) and 7(d') and Figs. 7(n) and 7(n'), respectively. This means that the theoretical chromatograms in Figs. A3(a), A3(a'), A4(a), and A4(a') represent those in Figs. 7(d'), 7(n'), 7(d), and 7(n) which should be realized provided there is no longitudinal diffusion in the column, respectively.

It can be seen in Parts (a)-(d), (a')-(d') of both Figs. A3 and A4 how theoretical chromatograms calculated on the basis of both Eqs. (6) and (7) approach asymptotically those calculated by using Eqs. (A4a)-(A4c) with an increase in x', provided that Eqs. (A1)-(A3) are fulfilled. Further, chromatograms that are virtually identical with those shown in Parts (d) and (d') of both Figs. A3 and A4 can be calculated by using both Eqs. (6) and (7) when $x' = 2000$.

In Ref. *11* the total shape of the theoretical chromatogram was argued on the basis of Eqs. (A9a)-(A9c) (to be precise, the relative expression of Eqs. (A9a)-(A9c); see Eq. 77 in Ref. *11*) rather than Eqs. (A4a)-(A4c). By comparing Parts (d) and (d') (obtained on the basis of Eqs. A4a-A4c) and Parts (e) and (e') (obtained on the basis of Eq. A9) of both Figs. A3 and A4, it can be understood that the total shape of the theoretical chromatogram is conserved nearly constant despite the approximation by Eqs. (A9a)-(A9c) for Eqs. (A4a)-(A4c) although the elution molarity changes considerably; this assures the validity of the argument made in Ref. *11*. [It should be noted that Figs. A3(e), A3(e'), A4(e), and A4(e') correspond to Figs. A10, A14, A11, and A15 in Ref. *11*, Appendix III, respectively.]

Acknowledgments

The authors thank Miss Y. Kobayashi and Mr. W. Kobayashi for carrying out some experiments.

REFERENCES

1. T. Kawasaki, *J. Chromatogr., 161,* 15 (1978).
2. T. Kawasaki, *Sep. Sci. Technol., 17,* 575 (1982).
3. T. Kawasaki, *Ibid., 17,* 1397 (1982).
4. T. Kawasaki, *Ibid., 22,* 121 (1987).
5. T. Kawasaki, *Ibid., 23,* 451 (1988).
6. T. Kawasaki, *Ibid., 23,* 2365 (1988).
7. T. Kawasaki, *J. Chromatogr., 82,* 167 (1973).
8. T. Kawasaki, *Ibid., 82,* 191 (1973).
9. T. Kawasaki, *Ibid., 82,* 241 (1973).
10. T. Kawasaki, *Ibid., 93,* 257 (1974).
11. T. Kawasaki, *Sep. Sci. Technol., 24,* 1109 (1989).
12. T. Imoto, L. N. Johnson, A. C. T. North, D. C. Phillips, and J. A. Pulpley, in *The Enzymes,* Vol. 7 (P. D. Boyer, H. Lardy, and K. Myrbäck, eds.), Academic, New York, 1972, p. 692.
13. T. Kawasaki, S. Takahashi, and K. Ikeda, *Eur. J. Biochem., 152,* 361 (1985).
14. T. Kawasaki and S. Takahashi, *Sep. Sci. Technol., 23,* 193 (1988).
15. T. Kawasaki, *Ibid., 23,* 601 (1988).
16. T. Kawasaki, *Ibid., 23,* 617 (1988).
17. T. Kawasaki, *Ibid., 23,* 1105 (1988).
18. T. Kawasaki, W. Kobayashi, K. Ikeda, S. Takahashi, and H. Monma, *Eur. J. Biochem., 157,* 291 (1986).
19. T. Kawasaki, M. Niikura, S. Takahashi, and W. Kobayashi, *Biochem. Int., 13,* 969 (1986).
20. T. Kawasaki, M. Niikura, and Y. Kobayashi, *J. Chromatogr.,* In Press.
21. T. Kawasaki, *Sep. Sci. Technol., 17,* 407 (1972).
22. K. A. Piez, in *Treatise on Collagen,* Vol. 1 (G. N. Ramachandran, ed.), Academic, New York, 1967, p. 267.

Received by editor December 12, 1988